

# Atomic Layer Deposition of Aluminum Oxide in Mesoporous Silica Gel

Jeffrey W. Elam,\* Joseph A. Libera, Trang H. Huynh, Hao Feng, and Michael J. Pellin

Argonne National Laboratory, Argonne, Illinois 60439

Received: April 5, 2010; Revised Manuscript Received: August 25, 2010

Silica gel is a mesoporous, granular material with a high specific surface area that is widely used as a support for heterogeneous catalysts. This study explores the atomic layer deposition (ALD) of aluminum oxide ( $\text{Al}_2\text{O}_3$ ) in silica gel. The coated materials were analyzed using weight-gain measurements, nitrogen adsorption surface-area analysis, energy dispersive X-ray analysis, and scanning electron microscopy. In addition, the individual ALD surface reactions on the silica gel powder were monitored in situ using quadrupole mass spectrometry. This study confirmed that the silica gel could be conformally coated using reactant exposure times of  $\sim 90$  s, and the surface area remained relatively unchanged even after 20  $\text{Al}_2\text{O}_3$  ALD cycles. EDAX measurements performed on silica gel specimens prepared using subsaturating trimethyl aluminum (TMA) exposures demonstrated that the spherical particles become infiltrated with the  $\text{Al}_2\text{O}_3$  ALD progressively from the outside of the particles to the core, and the kinetics of this process are dictated by the rapid consumption of TMA by the high surface area silica gel. The  $\text{Al}_2\text{O}_3$  ALD is inhibited on the silica gel surface for the first  $\sim 5$  ALD cycles, and this leads to a lower initial weight gain as well as a reduced proportion of methane released during the initial TMA exposures. This study provides useful insights into ALD processes on high surface area supports that will be valuable for the future development of nanostructured catalysts using ALD.

## Introduction

Silica gel is a granular, mesoporous material that is formed by acidifying an aqueous silicate solution and subsequently drying the precipitated gel. Silica gel is most commonly used as a desiccant and as the stationary phase in chromatographic separations columns but is also widely utilized as a support material for heterogeneous catalysts. As a catalyst support, silica gel offers a very high specific surface area (50–500  $\text{m}^2/\text{g}$ ) and the pore size, surface area, and particle size can be tailored to particular applications. Typically, catalytically active materials are introduced into the silica gel host using solution-based methods such as incipient wetness impregnation but vapor-phase methods including atomic layer deposition (ALD) are sometimes employed as well. This study explores the infiltration of silica gel with aluminum oxide ( $\text{Al}_2\text{O}_3$ ) using ALD.

ALD is a thin-film growth method that utilizes alternating, self-limiting reactions between gaseous precursors and a solid surface to deposit material in an atomic layer-by-layer fashion.<sup>1</sup> ALD is well suited to coating nanoporous solids because diffusion of the precursor vapors along with saturation of the individual surface reactions ensure that all surfaces of the porous material become uniformly coated by the ALD film. Consequently, a wide variety of nanoporous materials have been successfully coated by ALD including anodic aluminum oxide,<sup>2,3</sup> aerogels,<sup>4,5</sup> nanopowders,<sup>6</sup> and silica gel.<sup>7–12</sup> The very high specific surface area of silica gel enables detailed investigations of ALD surface chemistry using bulk-sensitive analytical techniques.<sup>13</sup> In addition, the high aspect ratio of the nanopores is challenging to the ALD precursors and therefore provides an excellent test of the self-limiting nature of the precursors.<sup>14</sup> Silica gel has been used extensively as a support material to prepare metal oxide catalysts by ALD including  $\text{TiO}_2$ ,<sup>7,8</sup>  $\text{Al}_2\text{O}_3$ ,<sup>9,10</sup>  $\text{ZrO}_2$ ,<sup>11</sup> and  $\text{V}_2\text{O}_5$ .<sup>12</sup> Recently, we studied the ALD of  $\text{ZnO}$  in silica gel.<sup>15</sup>

Aluminum oxide ( $\text{Al}_2\text{O}_3$ ) is a widely used catalyst and also catalyst support material. The TMA/ $\text{H}_2\text{O}$  process for  $\text{Al}_2\text{O}_3$  ALD has been studied extensively and is a well-characterized and well-

understood ALD process<sup>16</sup> and therefore was ideal for this investigation. ALD has been used previously to coat silica gel with  $\text{Al}_2\text{O}_3$  using both  $\text{AlCl}_3/\text{H}_2\text{O}$ <sup>10</sup> and TMA/ $\text{H}_2\text{O}$ .<sup>9</sup> Furthermore, the surface chemistry of TMA on silica gel has been studied using FTIR and other surface-sensitive techniques.<sup>10,17,18</sup>

In this investigation, we explored the ALD of  $\text{Al}_2\text{O}_3$  on silica gel powder. Weight-gain measurements were performed to establish the appropriate exposure conditions to saturate the ALD  $\text{Al}_2\text{O}_3$  surface reactions and to examine the nucleation and growth on the silica gel support. Nitrogen adsorption measurements were used to determine the surface area of the silica gel powder before and after coating by  $\text{Al}_2\text{O}_3$  ALD. Cross-sectional energy dispersive X-ray analysis (EDAX) was utilized to study the infiltration of the silica gel at various stages of the  $\text{Al}_2\text{O}_3$  ALD. We used these measurements to identify the rate-limiting factor governing  $\text{Al}_2\text{O}_3$  ALD in silica gel. We also employed in situ quadrupole mass spectrometry (QMS) to monitor the nucleation and growth of the ALD  $\text{Al}_2\text{O}_3$  on the silica gel surface. Although QMS measurements have been used previously to examine ALD reaction mechanisms on planar surfaces<sup>19</sup> and as a process monitor for coating powders,<sup>20</sup> this study presents the first application of QMS to explore ALD nucleation and growth on porous surfaces. We anticipate that insight gained from this detailed examination of the well-characterized TMA/ $\text{H}_2\text{O}$  process in silica gel will assist in the understanding of less familiar ALD systems in porous media, especially those systems relevant to heterogeneous catalysis.<sup>21,22</sup>

## Experimental Section

The ALD experiments used a hot-walled, viscous flow reactor constructed from a circular, stainless steel flow tube with an inside diameter of 5 cm.<sup>23</sup> Ultrahigh purity (99.999%) nitrogen carrier gas continuously passed through the flow tube at a mass flow rate of 360 sccm and a pressure of 1 Torr. The nitrogen was further purified using an Aeronex GateKeeper inert gas filter. The commercial silica gel used in this study was Silicycle

S10040 M with a specific surface area of 99.6 m<sup>2</sup>/g, a primary particle size of 75–200  $\mu\text{m}$ , and a nominal pore diameter of 30 nm. One gram of the silica gel was spread onto the bottom of a stainless steel tray and covered by a stainless steel wire cloth to contain the powder.<sup>15</sup> This method is likely to be inefficient compared to commercial ALD systems in which the carrier gas flows through the silica gel bed<sup>13</sup> but is adequate for this exploratory study.

Al<sub>2</sub>O<sub>3</sub> ALD was performed at a temperature of 150 °C using alternating exposures to trimethylaluminum (TMA, Aldrich, 95%) and deionized water (18 M $\Omega$  cm). Prior to coating, the silica gel was cleaned using a 10 min exposure to ozone produced by a commercial ozone generator (Ozone Engineering L11) using a feed of ultrahigh purity oxygen at a flow rate of 400 sccm to produce  $\sim 10\%$  ozone in oxygen. The Al<sub>2</sub>O<sub>3</sub> ALD timing sequences can be expressed as t1–t2–t3–t4 where t1 is the TMA exposure time, t2 is the purge time following the TMA exposure, t3 is the H<sub>2</sub>O exposure time, and t4 is the purge time following the H<sub>2</sub>O exposure where the units are seconds (s). The typical timing sequence for these studies was 90–180–90–180. During the reactant exposures, the partial pressures of the TMA and H<sub>2</sub>O reactants were  $\sim 0.15$  Torr as determined using a Baratron capacitance manometer pressure gauge.

The quantity of ALD Al<sub>2</sub>O<sub>3</sub> deposited on the silica gel was determined by direct weight measurements performed before and after the ALD coating using an analytical balance with a precision of 0.5 mg. Cross-sectional specimens for scanning electron microscopy (SEM, Hitachi S4700 with field emission gun electron beam source) and energy dispersive analysis of X-rays (EDAX) were prepared by embedding a small quantity of the coated silica gel in a conductive epoxy. The surface of the casting was then ground and polished to expose cross sections of the embedded silica particles on the polished surface. Next, a thin layer of electrically conductive carbon was evaporated onto the samples to reduce charging in the SEM. These samples were imaged in the SEM and EDAX analysis was performed to acquire 2D maps of the elemental composition for Si, O, and Al. The attenuation depth of X-rays generated by the electron beam in the sample was no more than 1  $\mu\text{m}$  for the highest energy X-ray (Si K) so that the EDAX maps are little affected by the depth of the  $\sim 100$   $\mu\text{m}$  diameter particle over most of the area of the particles.

The ALD reactor was equipped with a quadrupole mass spectrometer (QMS, Stanford Research Systems RGA300) located in a differentially pumped chamber separated from the reactor tube by a 20  $\mu\text{m}$  orifice and evacuated using a 50 L/s turbomolecular pump. The methane released during the Al<sub>2</sub>O<sub>3</sub> ALD surface reactions on the silica gel powder was monitored by recording the signal at mass-to-charge ratio  $m/e = 16$  versus time during individual TMA and H<sub>2</sub>O half reactions. The background QMS signals at  $m/e = 16$  generated by other surfaces in the ALD reactor as well as by cracks of the TMA and H<sub>2</sub>O molecules were accounted for by subtracting the  $m/e = 16$  signals recorded without silica gel in the reactor.

## Results and Discussion

**A) Weight-Gain and Surface-Area Measurements.** Our initial measurements were performed to establish the necessary saturation exposure conditions for the Al<sub>2</sub>O<sub>3</sub> ALD on silica gel in our ALD reactor. The solid circles in Figure 1 show the results of weight-gain measurements performed on 1 g silica gel samples after coating with 5 cycles of ALD Al<sub>2</sub>O<sub>3</sub> using the timing sequence x–180–90–180 in which the TMA exposure

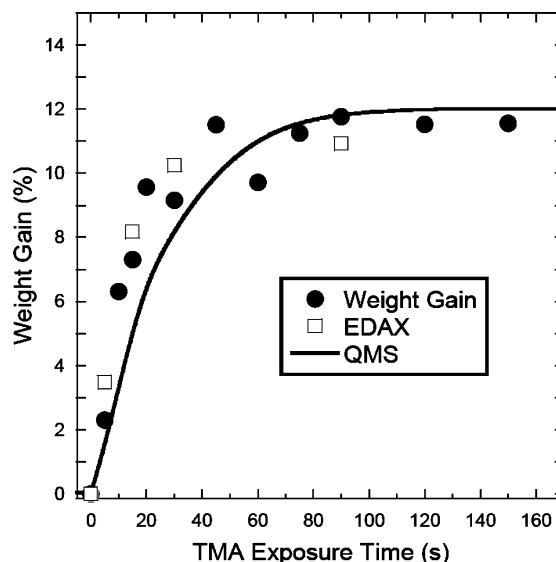


**Figure 1.** Measurements of Al<sub>2</sub>O<sub>3</sub> ALD saturation versus TMA exposure time performed on 1 g samples of silica gel obtained from weight-gain measurements (solid circles), EDAX measurements (open squares), and integrated QMS measurements (solid line).

time was varied between 0–150 s. Figure 1 shows that the weight gain increases with exposure time below  $\sim 90$  s after which the weight gain saturates at  $\sim 12\%$ . Additional weight-gain measurements varying the H<sub>2</sub>O exposure time (not shown) verified that the 90 s H<sub>2</sub>O exposures were sufficient to ensure saturation. Under the pressure and flow conditions in our system, the saturation exposure time of 90 s corresponds to  $2.3(\pm 0.4) \times 10^{-3}$  mol TMA. In contrast, only  $7.4(\pm 0.7) \times 10^{-4}$  mol TMA are required to saturate the surface of 1 g silica gel assuming a growth rate of 1.29 Å/cycle<sup>24</sup> so that only  $\sim 1/3$  of the TMA was utilized. We expect that precursor utilization could be increased by reducing the flow rate.

Next, the ALD Al<sub>2</sub>O<sub>3</sub> timing sequence was held constant at 90–180–90–180 and the number of exposures was varied between 1 and 20 cycles. The results of weight-gain measurements performed on these samples are shown by the solid circles in Figure 2. Figure 2 reveals that the ALD Al<sub>2</sub>O<sub>3</sub> weight gain increased at a low rate of 2.7%/cycle between 1 and 5 cycles, and then transitioned to a higher growth rate of 3.6%/cycle between 6 and 20 cycles. The lower growth rate below  $\sim 5$  ALD Al<sub>2</sub>O<sub>3</sub> cycles suggests that the Al<sub>2</sub>O<sub>3</sub> growth is inhibited on the silica gel surface.

The linear growth above 5 ALD Al<sub>2</sub>O<sub>3</sub> cycles is expected for an ALD process on a substrate with a constant surface area. In agreement with this expectation, the Brunauer–Emmett–Teller (BET) surface-area measurements performed on the silica gel specimens after different numbers of cycles and shown in Figure 3 demonstrate that the surface area of the silica gel remained relatively constant following the Al<sub>2</sub>O<sub>3</sub> ALD. One might expect the surface area to decrease if the silica gel pores became filled by the ALD Al<sub>2</sub>O<sub>3</sub>. Alternatively, the surface area should increase if the diameter of the primary silica gel particles increased with increasing ALD Al<sub>2</sub>O<sub>3</sub> thickness. The fact that the surface area remained essentially constant between 1–20 cycles suggests that either both of these effects are insignificant or that they cancel out.

It is instructive to compare these surface-area and weight-gain results with our previous observations for coating aerogel samples. Previously we measured a quadratic increase in percent weight gain versus number of cycles for ZnO ALD on silica

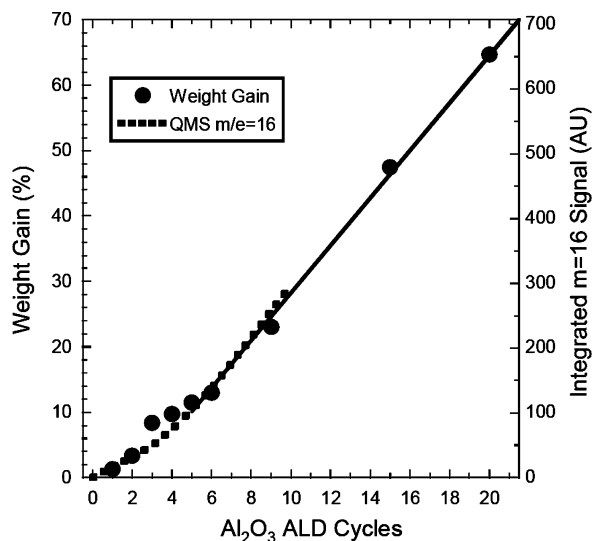


**Figure 2.** Quantity of  $\text{Al}_2\text{O}_3$  deposited versus number of ALD cycles performed on 1 g samples of silica gel obtained from weight-gain measurements (solid circles), and integrated QMS measurements (dashed line). Solid line shows linear least-squares fit to weight-gain measurements between 6 and 20  $\text{Al}_2\text{O}_3$  ALD cycles.

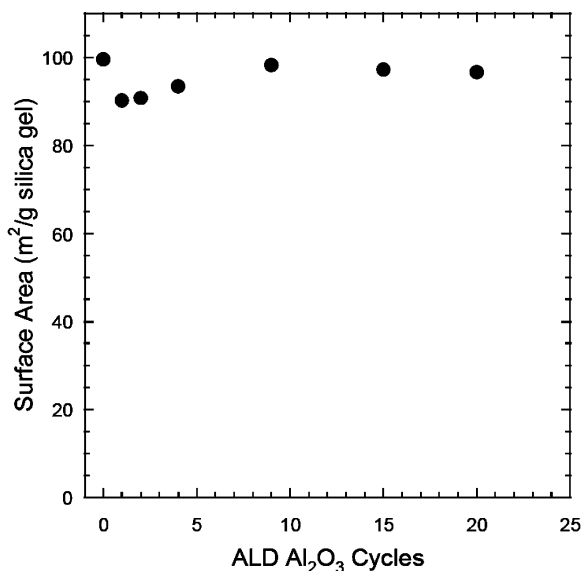


**Figure 3.** Surface area of  $\text{Al}_2\text{O}_3$  coated silica gel samples versus number of  $\text{Al}_2\text{O}_3$  ALD cycles determined by nitrogen adsorption using the BET method.

aerogel<sup>25</sup> and for W ALD on carbon aerogel.<sup>4</sup> We attributed this behavior to an increase in surface area of the aerogel samples with number of ALD cycles. The ALD ZnO and W films increased the diameter of the filaments linearly, and this yielded a quadratic increase in surface area. In agreement with this idea, BET surface-area measurements performed on the carbon aerogel specimens versus the number of W ALD cycles showed an increase in surface area with W thickness.<sup>4</sup>

The different behavior observed when coating the silica gel as compared with the aerogel samples is due to the fact that the initial diameter of the silica gel primary particles ( $\sim 30$  nm) is much larger than the initial diameters of the silica aerogel filaments ( $\sim 2$  nm) and the carbon aerogel filaments ( $\sim 10$  nm). Also, in the case of W ALD on carbon aerogel, the weight gain saturated following the deposition of 6 nm W, and this saturation was attributed to a plugging of the pores in the aerogel such that the W ALD precursors could no longer infiltrate the

material. This effect was not observed in the present study, suggesting that the pores of the silica gel remained open throughout the 20  $\text{Al}_2\text{O}_3$  ALD cycles, or approximately 2.6 nm  $\text{Al}_2\text{O}_3$ . The relatively constant silica gel surface area shown in Figure 3 also demonstrates that the silica gel pore structure remained open throughout the  $\text{Al}_2\text{O}_3$  ALD.

The average  $\text{Al}_2\text{O}_3$  weight gain deposited per cycle after 6 cycles is 3.6%. We can calculate the expected amount of  $\text{Al}_2\text{O}_3$  from the initial surface area of the silica gel ( $99.6 \text{ m}^2/\text{g}$ ), the  $\text{Al}_2\text{O}_3$  ALD growth rate measured on planar surfaces ( $1.29 \text{ \AA}/\text{cycle}$ ), and the density of ALD  $\text{Al}_2\text{O}_3$  ( $2.9 \text{ g}/\text{cm}^3$ )<sup>26</sup> to be 3.75%. The predicted  $\text{Al}_2\text{O}_3$  weight gain per cycle is very close to the experimentally determined value indicating that  $\text{Al}_2\text{O}_3$  ALD on the high surface area, nanoporous silica gel powder occurs at the same rate as on planar silicon using much smaller reactant exposures.

**B) EDAX Measurements.** To quantify the infiltration of the silica gel by the ALD  $\text{Al}_2\text{O}_3$ , cross sectional specimens of individual silica gel grains were analyzed using SEM and EDAX. The images in Figure 4 were acquired from a silica gel grain that had been coated using 9  $\text{Al}_2\text{O}_3$  ALD cycles with the timing sequence 90–180–90–180. The SEM secondary electron image (labeled SE) shows that the silica gel grain has a diameter of  $\sim 100 \mu\text{m}$ . The circle inside of the grain located below and right of the center is a void in the silica gel particle. These voids are typical and evidently arise during the manufacturing process. The images labeled Si K and O K are maps of the  $\text{K}\alpha$  X-ray intensity for Si and O, respectively. These maps appear uniform as expected because the silica gel particles are uniform in composition. The image labeled Al K is a map of the aluminum  $\text{K}\alpha$  X-ray intensity and is also very uniform in intensity. This image demonstrates qualitatively that the ALD  $\text{Al}_2\text{O}_3$  uniformly infiltrated the silica gel particles when the exposure times were sufficiently long to ensure saturation as determined from the weight-gain measurements in Figure 1. To quantify the EDAX intensity maps in Figure 4, these data sets were radially integrated to obtain 2D plots as shown in Figure 5. The Si, O, and Al intensities are very uniform from the edge of the silica gel particle at  $0 \mu\text{m}$  all the way to the center at  $\sim 45 \mu\text{m}$ . The Al trace in Figure 4 is a quantitative demonstration that the ALD  $\text{Al}_2\text{O}_3$  penetrated to the core of the silica gel particles.

Cross-sectional EDAX measurements similar to those shown in Figures 4 and 5 were made to determine the spatial distribution of the  $\text{Al}_2\text{O}_3$  at various stages of saturation. A series of silica gel samples were coated using 5 ALD  $\text{Al}_2\text{O}_3$  cycles with the timing sequence  $x$ –180–90–180 where  $x = 5, 15, 30$ , and 90s. The results of these measurements are shown in Figure 6. Using 5 s TMA exposures, the Al appears as a thin shell on the outer perimeter of the silica gel particles. For progressively longer TMA exposure times of 15 and 30 s, the Al signal extends further toward the core and at 90s, the Al EDAX signal extends fully to the middle of the particle. This behavior is quantified by the radially integrated Al EDAX profiles in Figure 7, which clearly show that the ALD  $\text{Al}_2\text{O}_3$  boundary moved progressively deeper into the silica gel particles with increasing exposure time.

The relative amount of  $\text{Al}_2\text{O}_3$  deposited using the different TMA exposure times can be calculated by integrating the linescan data in Figure 7 using an  $r^3$  weighting factor where  $r$  is the radial distance from the center of the silica gel particle. This weighting factor accounts for the fact that the Al signals in Figure 7 represent  $\text{Al}_2\text{O}_3$  deposited in concentric shells inside of the silica gel particle. The results of these weighed integration



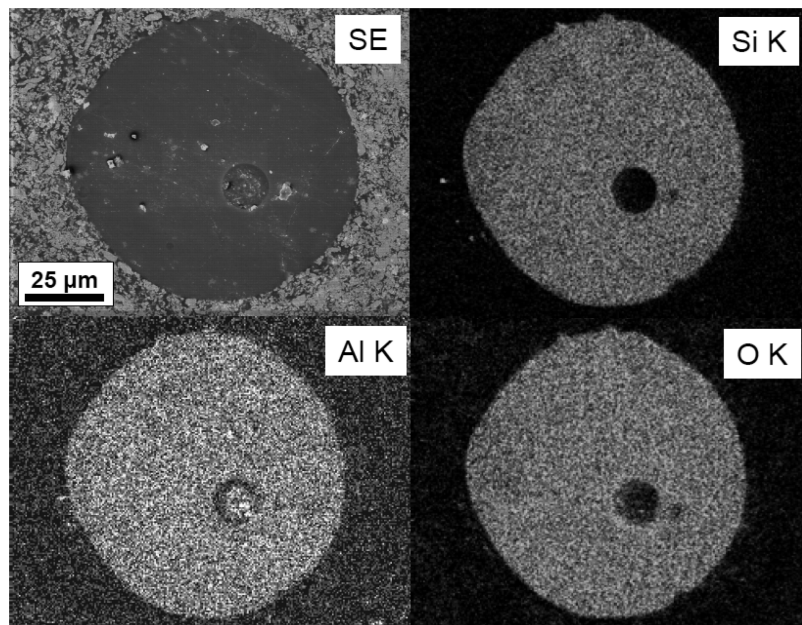


**Figure 4.** EDAX elemental maps of Si, O, and Al along with the corresponding secondary electron (SE) image for ALD  $\text{Al}_2\text{O}_3$  coated silica gel particle embedded and polished to reveal a hemispherical cross-section. The reactant exposures were 90 s.

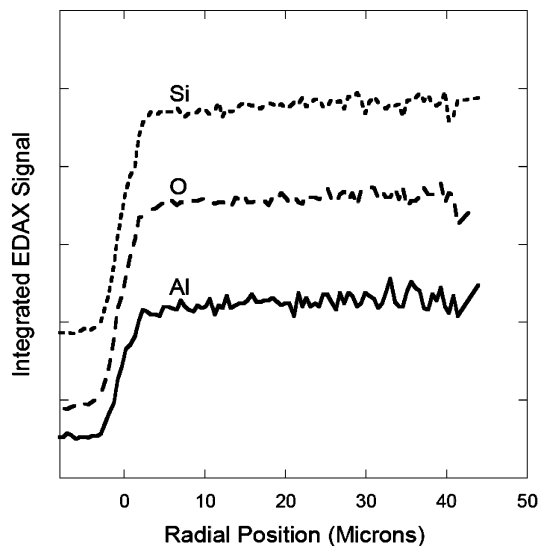


**Figure 5.** Element distribution profiles obtained by radial integration of the EDAX elemental maps in Figure 4. The traces are offset in the vertical direction for clarity.

calculations are shown as the open squares in Figure 1, where the EDAX measurements have been normalized to the weight-gain measurements. The EDAX measurements overlay the weight-gain measurements, indicating that both methods are viable for tracking the ALD infiltration of the silica gel.

Figure 1 shows that, before the coverage approaches saturation (0–20 s), the weight gain and EDAX measurements increase linearly with exposure time. A linear dependence of coverage on exposure time can result during ALD in porous materials when the reactive sticking coefficient is very small.<sup>2</sup> However, in this case the surface sites along each pore should fill randomly with time because the probability that a precursor molecule will diffuse to an empty site is much larger than the probability for reaction on that site. This is clearly not the case in our experiments because the reactive sites in the silica gel spheres fill sequentially from the outside to the center (Figures 6 and 7). This behavior clearly shows that reaction is much faster than diffusion. Instead, the initial linear growth in Figure

1 can be explained by the limited transport of the TMA so that a majority of the TMA supplied to the silica gel was consumed. During the initial 20 s of the TMA exposures,  $5.1(\pm 1) \times 10^{-4}$  mol TMA were supplied and the weight-gain measurements indicate that  $4.9(\pm 0.5) \times 10^{-4}$  mol TMA were consumed. This close correspondence supports the explanation that the rate of mass uptake was limited by the rate of precursor delivery in our experiments.

**C) In Situ Quadrupole Mass Spectrometry.** To explore the nucleation and growth of the ALD  $\text{Al}_2\text{O}_3$  on the nanoporous silica gel, in situ quadrupole mass spectrometry (QMS) was used to measure the  $\text{CH}_4$  gas-phase reaction product of the  $\text{Al}_2\text{O}_3$  ALD.<sup>27</sup> Part a of Figure 8 shows the results of QMS measurements performed while monitoring the  $\text{CH}_4$  signal at  $m/e = 16$  during a TMA exposure after several ALD  $\text{Al}_2\text{O}_3$  cycles ending with a  $\text{H}_2\text{O}$  exposure. The upper trace in part a of Figure 8 results from measurements performed with 1 g silica gel installed in the ALD reactor, whereas the lower trace results from an identical measurement performed without the silica gel. The  $m/e = 16$  signal observed for the empty reactor arose from several sources including the crack of the TMA molecule, and  $\text{CH}_4$  produced from  $\text{Al}_2\text{O}_3$  ALD on the reactor surfaces and surfaces in the differentially pumped region of the mass spectrometer. By subtracting the empty reactor signal from the signal obtained with the silica gel installed, we are left with the signal originating solely from the silica gel, and this data is shown in part b of Figure 8.

Part b of Figure 8 shows that the  $\text{CH}_4$  produced by TMA reaction with the hydroxylated silica gel surface was at a maximum at the start of the TMA pulse and then gradually decayed over  $\sim 60$  s. By plotting the integral of the data in part b of Figure 8 versus time, we obtain the solid curve in Figure 1, which is scaled to match the intensity of the weight-gain measurements. As shown in Figure 1, the integrated  $m/e = 16$  signal agrees very well with the weight-gain and EDAX measurements. This agreement demonstrates that the in situ QMS measurements accurately probe the silica gel infiltration kinetics.

The  $m/e = 16$  QMS signal from  $\text{CH}_4$  was recorded during all of the TMA and  $\text{H}_2\text{O}$  exposures for 10 ALD  $\text{Al}_2\text{O}_3$  cycles

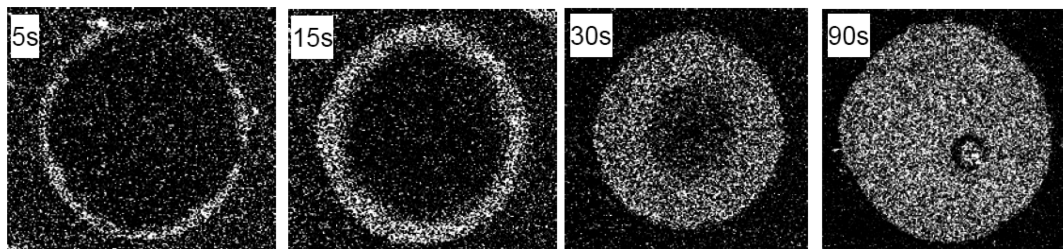


**Figure 6.** EDAX elemental maps for Al obtained from polished cross sections of silica gel following  $\text{Al}_2\text{O}_3$  ALD using TMA exposure times of 5, 15, 30, and 90 s.

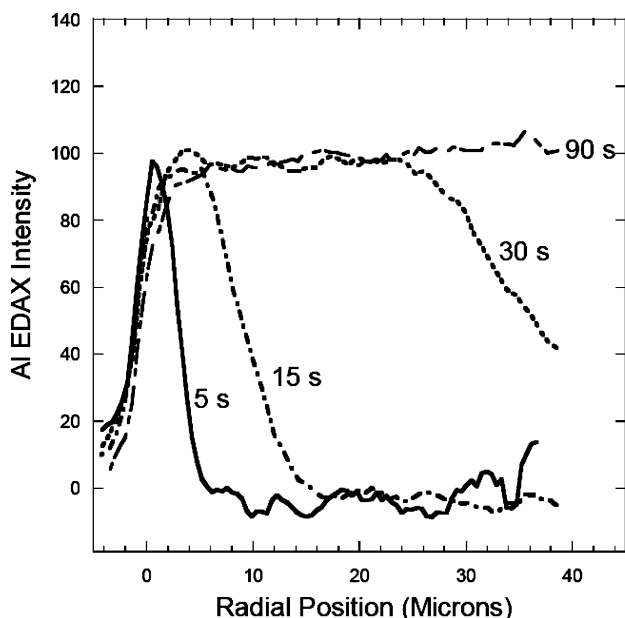


**Figure 7.** Aluminum distribution profiles obtained by radial integration of the EDAX elemental maps in Figure 6.

beginning on a fresh 1.0 g silica gel sample. The integrated  $m/e = 16$  signals from these measurements are shown in Figure 9 where the solid circles show the measurements performed during the TMA reactions and the open squares show the measurements performed during the  $\text{H}_2\text{O}$  reactions. Figure 9

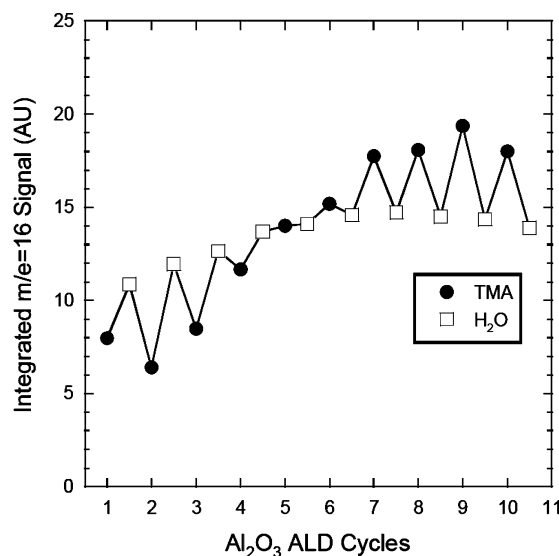


**Figure 9.** Integrated  $m/e = 16$  QMS signals recorded during individual TMA exposures (solid circles) and  $\text{H}_2\text{O}$  exposures (open squares) for first 10 cycles of  $\text{Al}_2\text{O}_3$  ALD on silica gel.

shows that the integrated  $m/e = 16$  signal increases initially for the first 6–7 cycles before reaching a plateau at a constant value. In addition, the  $\text{CH}_4$  QMS signals oscillate in intensity with each TMA or  $\text{H}_2\text{O}$  exposure. Initially the  $\text{CH}_4$  QMS signals are larger during the  $\text{H}_2\text{O}$  exposures but this pattern gradually evolves such that after 6 cycles the  $\text{CH}_4$  QMS signals are larger during the TMA exposures. This behavior is seen clearly in

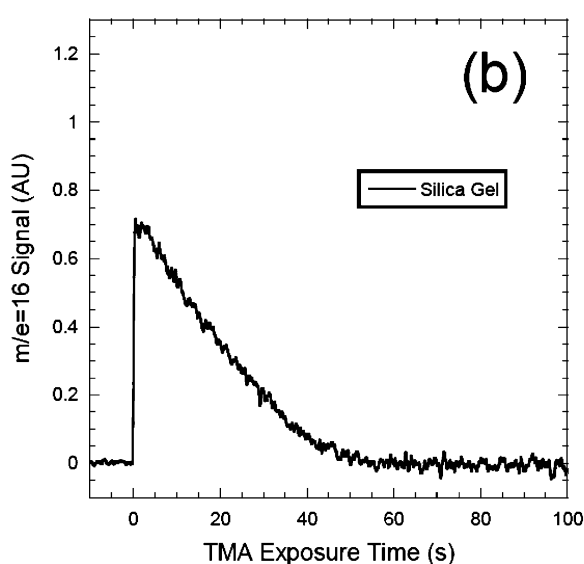
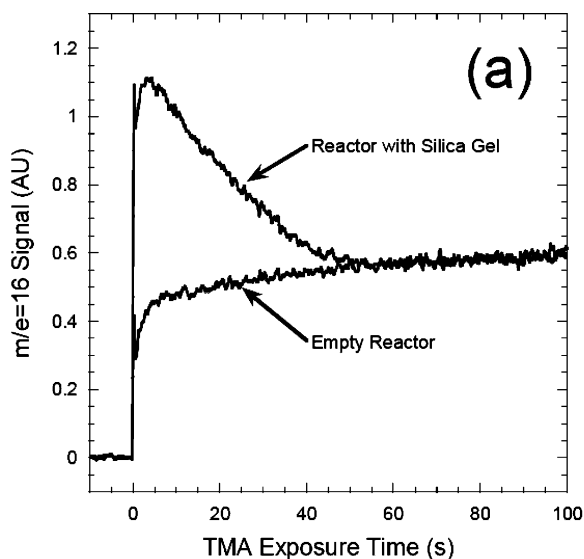


**Figure 8.** (a) QMS signal for  $m/e = 16$  (methane) recorded during TMA exposure on a  $\text{H}_2\text{O}$ -treated  $\text{Al}_2\text{O}_3$  surface with 1 g silica gel installed in reactor (upper trace) and with empty reactor (lower trace). (b) Difference between reactor with silica gel signal and empty reactor signals in part a of Figure 9.

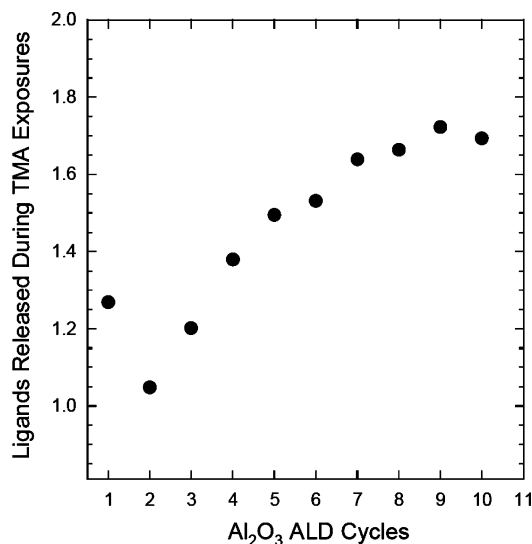


**Figure 10.** Average number of ligands released during TMA exposures for Al<sub>2</sub>O<sub>3</sub> ALD versus ALD cycles.

Figure 10, which plots the average number of ligands released from each TMA molecule during the TMA exposures, which is calculated using:  $y = 3A/(A + B)$ , where  $A$  and  $B$  are the integrated  $m/e = 16$  signals recorded during the TMA and H<sub>2</sub>O exposures, respectively. Figure 10 demonstrates that  $y$  increases with ALD cycles from an initial value of  $\sim 1.2$  to a final value of  $\sim 1.7$  after 10 cycles. This evolution is consistent with an increase in the density of surface hydroxyl groups as described below. In addition, the final value of  $y \sim 1.7$  is in good agreement with previous in situ QMS and quartz crystal microbalance measurements of Al<sub>2</sub>O<sub>3</sub> ALD performed on planar surfaces at this temperature.<sup>27</sup>

The sum of the  $m/e = 16$  signals during the TMA and H<sub>2</sub>O exposures of each cycle is proportional to the amount of Al<sub>2</sub>O<sub>3</sub> deposited in that cycle. By summing these values, we obtain a quantity that is proportional to the thickness of the Al<sub>2</sub>O<sub>3</sub> film. The summed  $m/e = 16$  signals are shown as the dashed line in Figure 2. The QMS data in Figure 2 demonstrate that the Al<sub>2</sub>O<sub>3</sub> growth per cycle increased for the first 6–7 cycles before reaching a constant value in agreement with the weight-gain measurements. This agreement lends credence to our mechanistic interpretations of the QMS signals.

The gradual increase in growth per cycle over the first 6–7 cycles resembles “Type I” substrate-inhibited growth as has been seen previously for Al<sub>2</sub>O<sub>3</sub> ALD on chemical SiO<sub>2</sub> surfaces.<sup>16,28</sup> The Al<sub>2</sub>O<sub>3</sub> growth rate is determined in part by the OH group density on the surface.<sup>16,29</sup> One possible cause for this is a lower OH group density on the silica gel surface as compared to the ALD Al<sub>2</sub>O<sub>3</sub> surface at the deposition temperature of 200 °C. On SiO<sub>2</sub>, the OH group density is  $\sim 6.3 \text{ nm}^{-2}$ , whereas on Al<sub>2</sub>O<sub>3</sub> the OH group density is  $\sim 8.5 \text{ nm}^{-2}$ .<sup>30,31</sup> The OH density ratio for these two surfaces is thus  $8.5/6.3 = 1.35$ . From Figure 9, the combined  $m/e = 16$  signals measured during the first TMA and H<sub>2</sub>O exposures is 19 and during the final cycle is 32. The ratio of these values,  $32/19 = 1.7$ , is in fair agreement with the OH density ratio on the SiO<sub>2</sub> and Al<sub>2</sub>O<sub>3</sub> surfaces.

Another possible explanation for the initially low Al<sub>2</sub>O<sub>3</sub> growth rate as well as the lower relative amount of CH<sub>4</sub> produced during the initial ALD cycles is surface poisoning by Si–CH<sub>3</sub>\* surface species. TMA can react equally well with both OH groups and bridge-bonded oxygen on silica.<sup>10,18</sup> When the TMA reacts on bridge-bonded oxygen, the resulting surface species are Si–O–Al(CH<sub>3</sub>)<sub>2</sub>\* and Si–CH<sub>3</sub>\*. These Si–CH<sub>3</sub>\*

species are difficult to remove during the water exposures and will prevent adsorption during subsequent ALD cycles on these locations. This mechanism was invoked previously to explain the hindered Al<sub>2</sub>O<sub>3</sub> growth on silica gel preheated to 600 °C.<sup>10</sup> In this previous study, the hindered growth was much more pronounced, but this is probably because the much higher pretreatment temperature produced a larger concentration of bridge-bonded oxygen species, which then increased the fraction of Si–CH<sub>3</sub>\* poisoned sites.

## Conclusions

This study confirms that Al<sub>2</sub>O<sub>3</sub> ALD, which is generally considered to be an ideal ALD process, follows very similar behavior in high surface area silica gel to that observed on planar silica surfaces. While not unexpected, this result establishes a useful basis for understanding the synthesis of more complex materials comprised of multiple layers and combining multiple ALD processes such as nanostructured catalysts.<sup>21,22</sup> We found that the silica gel could be conformally coated using reactant exposure times of  $\sim 90$  s in our apparatus and that the surface area remained relatively unchanged even after 20 Al<sub>2</sub>O<sub>3</sub> ALD cycles. Cross-sectional EDAX analysis of specimens prepared using subsaturating TMA exposures revealed that the spherical particles became infiltrated with the ALD Al<sub>2</sub>O<sub>3</sub> progressively from the outside of the particles to the core, and the dynamics of this process are dictated by the local, rapid consumption of TMA by the high surface area silica gel. We demonstrate that in situ QMS is a viable method for monitoring the nucleation and growth of ALD thin-film materials in porous media allowing mechanistic details to be inferred in a nonintrusive and nondestructive manner. The Al<sub>2</sub>O<sub>3</sub> ALD was inhibited on the silica gel surface for the first  $\sim 5$  ALD cycle leading to a lower initial weight gain as well as a reduced proportion of methane released during the initial TMA exposures consistent with previous studies of the Al<sub>2</sub>O<sub>3</sub> ALD surface chemistry on silica.

**Acknowledgment.** This work was supported by the U.S. Department of Energy, EERE-Industrial Technologies Program under FWP-49055, and the BES-Materials Sciences under Contract W-31-109-ENG-38. The electron microscopy was accomplished at the Electron Microscopy Center for Materials Research at Argonne National Laboratory, a U.S. Department of Energy Office of Science Laboratory operated under Contract No. DE-AC02-06CH11357 by UChicago Argonne, LLC. The authors are grateful to Dr. Angel Yanguas-Gil for helpful discussions concerning the infiltration kinetics.

## References and Notes

- (1) Ritala, M.; Leskela, M. Atomic Layer Deposition. In *Handbook of Thin Film Materials*; Nalwa, H. S., Ed.; Academic Press: San Diego, 2001; Vol. 1; pp 103.
- (2) Elam, J. W.; Routkevitch, D.; Mardilovich, P. P.; George, S. M. *Chem. Mater.* **2003**, *15*, 3507.
- (3) Pellin, M. J.; Stair, P. C.; Xiong, G.; Elam, J. W.; Birrell, J.; Curtiss, L.; George, S. M.; Han, C. Y.; Iton, L.; Kung, H.; Kung, M.; Wang, H. H. *Catal. Lett.* **2005**, *102*, 127.
- (4) Elam, J. W.; Libera, J. A.; Pellin, M. J.; Zinovev, A. V.; Greene, J. P.; Nolen, J. A. *Appl. Phys. Lett.* **2006**, *89*, 053124.
- (5) Kucheyev, S. O.; Biener, J.; Wang, Y. M.; Baumann, T. F.; Wu, K. J.; van Buuren, T.; Hamza, A. V.; Satcher, J. H.; Elam, J. W.; Pellin, M. J. *Appl. Phys. Lett.* **2005**, *86*, 083108.
- (6) Ferguson, J. D.; Weimer, A. W.; George, S. M. *Appl. Surf. Sci.* **2000**, *162–163*, 280.
- (7) Kol'tsov, S. I. *J. Appl. Chem. USSR* **1970**, *43*, 1976.
- (8) Haukka, S.; Lakomaa, E. L.; Jylha, O.; Vilhunen, J.; Hornytzkyj, S. *Langmuir* **1993**, *9*, 3497.
- (9) Kol'tsov, S. I.; Kopylov, V. B.; Smirnov, V. M.; Aleskovskii, V. B. *J. Appl. Chem. USSR* **1976**, *49*, 525.

- (10) Lakomaa, E.-L.; Root, A.; Suntola, T. *Appl. Surf. Sci.* **1996**, *107*, 107.
- (11) Kytokivi, A.; Lakomaa, E. L.; Root, A. *Langmuir* **1996**, *12*, 4395.
- (12) Keranen, J.; Guimon, C.; Iiskola, E.; Auroux, A.; Niinisto, L. *J. Phys. Chem. B* **2003**, *107*, 10773.
- (13) Haukka, S.; Lakomaa, E. L.; Suntola, T. Adsorption controlled preparation of heterogeneous catalysts. In *Adsorption and Its Applications in Industry and Environmental Protection, Vol I: Applications in Industry*; Dabrowski, A., Ed.; Elsevier: New York, 1999; Vol. 120; pp 715.
- (14) Haukka, S. *ALD Surface Reactions of Cu Precursors*; AVS Topical Conference on Atomic Layer Deposition, ALD2004, 2004; Helsinki, Finland.
- (15) Libera, J. A.; Elam, J. W.; Pellin, M. J. *Thin Solid Films* **2008**, *516*, 6158.
- (16) Puurunen, R. L. *J. Appl. Phys.* **2005**, *97*.
- (17) Yates, D. J. C.; Dembinski, G. W.; Kroll, W. R.; Elliot, J. J. *J. Phys. Chem.* **1969**, *73*, 911.
- (18) Bartram, M. E.; Michalske, T. A.; J. W. Rogers, J. *J. Phys. Chem.* **1991**, *95*, 4453.
- (19) Juppo, M.; Rahtu, A.; Ritala, M.; Leskela, M. *Langmuir* **2000**, *16*, 4034.
- (20) King, D. M.; Liang, X. H.; Burton, B. B.; Akhtar, M. K.; Weimer, A. W. *Nanotechnology* **2008**, *19*, 255604–255611.
- (21) Feng, H.; Elam, J. W.; Libera, J. A.; Setthapun, W.; Stair, P. C. *Chem. Mater.* **2010**, *22*, 3133–3142.
- (22) Stair, P. C.; Marshall, C.; Xiong, G.; Feng, H.; Pellin, M. J.; Elam, J. W.; Curtiss, L.; Iton, L.; Kung, H.; Kung, M.; Wang, H. H. *Top. Catal.* **2006**, *39*, 181.
- (23) Elam, J. W.; Groner, M. D.; George, S. M. *Rev. Sci. Instrum.* **2002**, *73*, 2981.
- (24) Elam, J. W.; Sechrist, Z. A.; George, S. M. *Thin Solid Films* **2002**, *414*, 43.
- (25) Elam, J. W.; Xiong, G.; Han, C. Y.; Wang, H. H.; Birrell, J. P.; Welp, U.; Hryn, J. N.; Pellin, M. J.; Baumann, T. F.; Poco, J. F.; Satcher, J. H. *J. Nanomaterials* **2006**, *2006*, 1.
- (26) Groner, M. D.; Fabreguette, F. H.; Elam, J. W.; George, S. M. *Chem. Mater.* **2004**, *16*, 639.
- (27) Rahtu, A.; Alaranta, T.; Ritala, M. *Langmuir* **2001**, *17*, 6506.
- (28) Zhao, C.; Brijs, B.; Dortu, F.; Gendt, S. D.; Caymax, M.; Heyns, M.; Besling, W.; Maes, J. W. *Proc.-Electrochem. Soc.* **2003**, *2003–3*, 243.
- (29) Ott, A. W.; Klaus, J. W.; Johnson, J. M.; George, S. M. *Thin Solid Films* **1997**, *292*, 135.
- (30) Puurunen, R. L.; Lindblad, M.; Root, A.; Krause, A. O. I. *Phys. Chem. Chem. Phys.* **2001**, *3*, 1093.
- (31) Puurunen, R. L.; Root, A.; Haukka, S.; Iiskola, E. I.; Lindblad, M.; Krause, A. O. I. *J. Phys. Chem. B* **2000**, *104*, 6599.

JP1030587